Response to Comments from Reviewer 2

We would like to thank the editor and referee for their comments and suggestions on the manuscript. We would also like to answer the questions raised by the report from the reviewer as following.

[Q1] In the updated text, the $L-\kappa_1$ phase diagram shows how the vortex cluster formation depends on the system size in the absence of impurity. The $g-\kappa_1$ phase diagram demonstrates how the presence of the impurities and their strength modify the cluster formation. However, it should be clarified how these diagrams were obtained, and, specifically, which criteria were used to distinguish the vortex lattice and cluster phases. The studied systems have only 10-15 vortices, and the authors should motivate how they distinguish the phases while working with such a small number of vortices. (Quoted from the report of Reviewer 2)

[A1] Following the reference [J.Y. Ge, J. Gutierrez, A. Lyashchenko, V. Filipov, J. Li and V.V. Moshchalkov, Direct visualization of vortex pattern transition in ZrB_{12} with Ginzburg-Landau parameter close to the dual point, Phys. Rev. B 90, 184511 (2014)], **we can determine the phase separation lines from the dependence of magnetization M on the Ginzburg-Landau (GL) parameter κ_1 in our investigations.** In the manuscript, we set the external magnetic field $H=0.8H_0$, where $H_0=\Phi_0/\left(2\pi\xi_1^2\right)$ represents the unit of magnetic field with the flux quantum $\Phi_0=\pi\hbar c/e$ and ξ_1 denotes the coherence length for the first band. **For the type-2 superconductor**, at small κ_1 the system will stay at the Meissner phase and give the magnetization $-4\pi M=H-\langle B\rangle\approx 0.8H_0$ due to the perfect diamagnetism, where $\langle B\rangle$ describes the average magnetic induction over the sample area S. While at large κ_1, the magnetic field penetrates the superconductor to form the Abrikosov vortex lattice and the magnetization will reduce gradually in a broad range of κ_1. **Thus, with the definition of $M'=\mathrm{d}M/\mathrm{d}\kappa_1$, it will show a discontinuous jump at the critical κ_1 of the phase transition from the perfect diamagnetic state to the vortex lattice state. For the type-1.5 superconductor**, at small κ_1 the sample remains in the Meissner state and M is still close to $0.8H_0$. With the increase of κ_1, the system first enters the vortex cluster phase and the magnetization will decrease linearly in a narrow range

of κ_1 exactly as in the case of the intermediate state of type-1 superconductors. As κ_1 is further raised, we will observe the vortex lattice phase, and the decline in M will exhibit a significant deceleration compared to the vortex cluster phase due to the dominance of short-range repulsive intervortex interaction. **In this circumstance, M' will display two discontinuous jumps at the critical points of the phase transitions from the perfect diamagnetic state to the vortex cluster state, and ultimately to the vortex lattice state.** This identification method is still applicable to systems with a relatively small number of vortices, see Fig. 1 on page 5 (in the absence of impurity) and Fig. 3 on page 7 (in the presence of impurity) in this Response as the specific examples of the discussions mentioned above. Also see the third paragraph on page 6 in the revised version of manuscript.

[Q2] In addition to that, the current version of the text does not provide any details about the method used to draw the phase separation lines. I recommend that the authors specify which points they check in the parameter space and explain how they extrapolate the results. (Quoted from the report of Reviewer 2)

[A2] **Based on the finite element method and COMSOL Multiphysics software, we now perform the detailed calculations on the phase separation lines both in the absence and presence of an isotropic impurity.** We start from the GL free energy functional of two-gap superconductors

$$F=\sum_i\left[-\alpha_i\left|\Psi_i\right|^2+\frac{\beta_i}{2}\left|\Psi_i\right|^4+\frac{1}{2m_i}\left|\left(-i\hbar\nabla-\frac{2e}{c}\mathbf{A}\right)\Psi_i\right|^2\right]+\frac{\mathbf{B}^2}{8\pi}\ . \tag{1}$$

Here Ψ_i $(i=1,2)$ represents the superconducting order parameter and m_i is the effective mass for each band. The coefficient α_i is a function of temperature, while β_i is independent of temperature. In the presence of the T_c disorder (T_c: the critical temperature), the parameters α_1 and α_2 can be approximately expressed as $\alpha_i=\alpha_{i0}g(\mathbf{r})$. Here we introduce a function $g(\mathbf{r})$ between -1 and $+1$ to model the defect potential which will deplete the superconducting state at specific positions. $\mathbf{B}=\nabla\times\mathbf{A}$ is the magnetic induction and $\mathbf{A}$ the vector potential.

Then, the time-dependent Ginzburg-Landau (TDGL) equations of the multi-component superconducting system can be derived from

$$-\Gamma_i\frac{\partial\Psi_i}{\partial t}=\frac{\delta F}{\delta\Psi_i^*}\qquad\text{and}\qquad-\sigma_n\frac{\partial\mathbf{A}}{\partial t}=\frac{\delta F}{\delta\mathbf{A}} \tag{2}$$

where Γ_i is the relaxation time of order parameters and σ_n represents the electrical conductivity of the normal sample in the two-band case. Therefore, minimization of the free energy F with respect to Ψ_i and $\mathbf{A}$ leads to the following dimensionless TDGL equations in the zero electrostatic potential gauge

$$-\Gamma_1 \frac{\partial \Psi_1}{\partial t} = -\left[g(\mathbf{r}) - \left|\Psi_1\right|^2 \right] \Psi_1 + \left(-\mathrm{i}\nabla - \mathbf{A}\right)^2 \Psi_1, \tag{3}$$

$$-\Gamma_2 \frac{\partial \Psi_2}{\partial t} = -\left[\frac{\alpha_{20}}{\alpha_{10}} g(\mathbf{r}) - \frac{\beta_2}{\beta_1} \left|\Psi_2\right|^2 \right] \Psi_2 + \frac{m_1}{m_2} \left(-\mathrm{i}\nabla - \mathbf{A}\right)^2 \Psi_2 \tag{4}$$

and

$$-\frac{\partial \mathbf{A}}{\partial t} = \kappa_1^2 \nabla \times \nabla \times \mathbf{A} - \mathbf{J}_s \tag{5}$$

with the supercurrent

$$\mathbf{J}_s = \left[\frac{\mathrm{i}}{2} (\Psi_1 \nabla \Psi_1^* - \Psi_1^* \nabla \Psi_1) - \left|\Psi_1\right|^2 \mathbf{A} \right] + \frac{m_1}{m_2} \left[\frac{\mathrm{i}}{2} (\Psi_2 \nabla \Psi_2^* - \Psi_2^* \nabla \Psi_2) - \left|\Psi_2\right|^2 \mathbf{A} \right]. \tag{6}$$

Here in the clean limit with the impurity function $g = 1$, we introduce the coherence length $\xi_i^2 = \hbar^2 / \left(2 m_i \alpha_{i0}\right)$, the London penetration depth $\lambda^{-2} = \lambda_1^{-2} + \lambda_2^{-2}$ with $\lambda_i^{-2} = 4\pi e^2 \Psi_{i0}^2 / (m_i c^2)$ and $\Psi_{i0} = \sqrt{\alpha_{i0} / \beta_i}$, and the GL parameter $\kappa_1 = \lambda_1 / \xi_1$. We then take the coordinate $\mathbf{r}$ in units of ξ_1, the time t in units of $t_0 = m_1 \sigma_n / \left(4 e^2 \Psi_{10}^2\right)$, Γ_i in units of $\alpha_{10} t_0$ and the order parameter Ψ_i in units of Ψ_{10}. We also set the magnetic induction $\mathbf{B}$ in units of $H_0 = \Phi_0 / \left(2\pi \xi_1^2\right)$ and the vector potential $\mathbf{A}$ in units of $A_0 = H_0 \xi_1$.

Based on the two-band TDGL equations (3)-(5), we can perform the numerical calculations on the variations of magnetization M with the GL parameter κ_1. We first split the order parameters into the real and imaginary parts, i.e. $\Psi_1 = u_1 + \mathrm{i} u_2$ and $\Psi_2 = u_3 + \mathrm{i} u_4$. With the external magnetic field $\mathbf{H} = H \hat{\boldsymbol{z}}$, we can set the magnetic induction $\mathbf{B} = B \hat{\boldsymbol{z}}$ inside the superconductor. Then, we can write the magnetic potential in component form as $\mathbf{A} = \left(u_5, u_6\right)$ on the *xy*-plane, and obtain $B = u_{6x} - u_{5y}$ from the relation $\mathbf{B} = \nabla \times \mathbf{A}$. Noting that the subscript x or y denotes the partial derivative with respect to the corresponding variable here. The magnetization which is defined as $-4\pi M = H - \langle B \rangle$ is a direct measure of the expelled external magnetic field from the superconducting system,

where $\langle B \rangle$ describes the average magnetic induction over the sample area S. In the procedure of simulations, we also set the coefficients in the GL equations as $\Gamma_1 = \Gamma_2 = 5$, $m_1 = 2m_2$, $\alpha_{10} = \alpha_{20}$ and $\beta_1 = \beta_2$.

In the absence of impurity, as an example, we choose $15\xi_1 \times 15\xi_1$ and $50\xi_1 \times 50\xi_1$ superconducting samples to determine the critical κ_1 in the phase transitions. We then plot the variations of M and its derivative with κ_1 at $t = 10^4 t_0$ in Fig. 1. From Fig. 1, we can observe that the $15\xi_1 \times 15\xi_1$ system exhibits the type-2 magnetic behavior. At small κ_1, the superconductor stays at the Meissner phase and the perfect diamagnetism leads to $-4\pi M \approx 0.8H_0$. While at large κ_1, the sample enters the vortex lattice phase and M reduces gradually in a broad range of κ_1. On the contrary, we can also see from Fig. 1 that the $50\xi_1 \times 50\xi_1$ system shows the type-1.5 superconducting properties. At small κ_1, the superconductor remains at the Meissner state and M is still close to $0.8H_0$. With the increase of κ_1, the magnetic field starts to penetrate the sample and the flux lines will exist in the form of the magnetic cluster due to the long-range attractive interaction between vortices, which induces a linear decrease of the magnetization in a narrow range of κ_1. As κ_1 is further raised, the number of vortices in the system continues to increase and eventually forms the stable Abrikosov flux lattice. In this circumstance, the rate of increase in vortex density will significantly slow down compared to the vortex cluster phase due to the dominance of short-range repulsive intervortex interaction. In order to accurately determine the critical points of the phase transitions, we further calculate the first-order derivative M' as a function of κ_1 in the inset of Fig. 1. It can be clearly observed that for the $15\xi_1 \times 15\xi_1$ superconductor, M' exhibits a discontinuous jump at $\kappa_1 = 1.48$, which denotes the transition of the system from the Meissner state to the vortex lattice state. For the $50\xi_1 \times 50\xi_1$ superconductor, M' shows two discontinuous jumps and the sample enters the vortex cluster phase at $\kappa_1 = 1.28$, then transfers to the vortex lattice phase at $\kappa_1 = 1.67$.

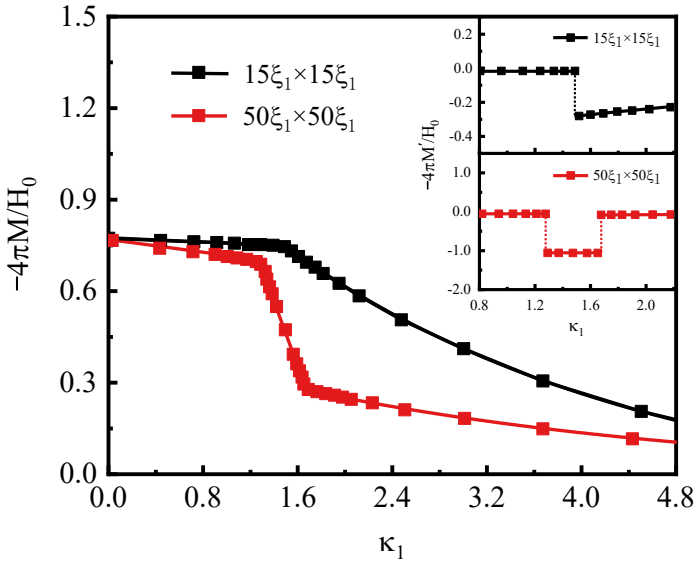

Figure 1: Variations of magnetization M (main) and its first-order derivative M' (inset) with GL parameter κ_1 for the $L\times L$ two-band superconductor in the absence of impurity. We set the external magnetic field $H=0.8H_0$ in the numerical simulations.

With this approach, we can further calculate the critical κ_1 for arbitrary value of L and obtain the $L-\kappa_1$ phase diagram as shown in Fig. 2. It can be seen from Fig. 2 that with the decrease of L, the vortex cluster phase produced by the long-range attractive interaction between vortices gradually vanishes. Meanwhile, we also notice the critical sample size L_c for the disappearance of this cluster state is $32\xi_1$. Thus, the superconducting system will stay in the type-1.5 regime above L_c and the type-2 regime below L_c in the absence of impurity. Also see the first paragraph, lines 1-2 of the second paragraph and Fig. 1 on page 7 in the revised version of manuscript.

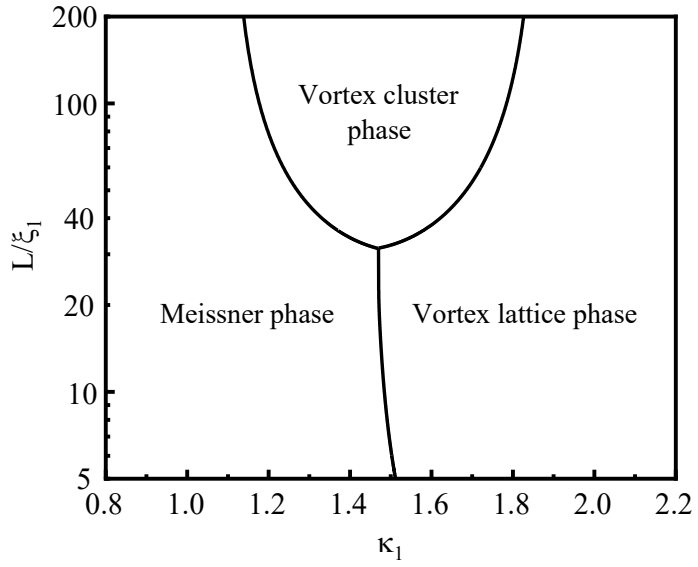

Figure 2: The $L-\kappa_1$ phase diagram of the $L\times L$ two-band superconductor in the absence of impurity. We set the external magnetic field $H=0.8H_0$ in the numerical simulations, and plot the sample size L on a logarithmic scale.

Now, we try to explore the possible generation of the vortex cluster phase in the mesoscopic superconducting system with $L<L_c$ due to the impurity effect. As an example, we introduce an isotropic impurity with the radius $0.5\xi_1$ at the center of the $15\xi_1\times15\xi_1$ superconducting sample here. With the T_c disorder model, the defect function $g(\mathbf{r})$ will be characterized by the disorder strength g inside the impurity. **We set the value of g as -0.1 and -0.5, and then plot the variations of M and its derivative with κ_1 at $t=10^4t_0$ in Fig. 3.** From Fig. 3, we can observe that for $g=-0.1$, this mesoscopic system exhibits the type-2 magnetic behavior. With the transition of the superconductor from the Meissner state to the vortex lattice state, the magnetization reduces gradually from the perfect diamagnetism $-4\pi M\approx0.8H_0$. Meanwhile, we can also see from Fig. 3 that for $g=-0.5$, the sample shows the type-1.5 superconducting properties. In the process of the transitions from the perfect diamagnetic state to the vortex cluster state, and ultimately to the vortex lattice state, the magnetization curve first remains close to $0.8H_0$, then decreases linearly in a narrow range of κ_1 and finally reduces with a relatively small extent compared to its neighboring phase. Furthermore, we can clearly observe from the inset of Fig. 3 that for $g=-0.1$, the phase transition from the Meissner state directly to the vortex lattice state

appears at $\kappa_1 = 1.38$. For $g = -0.5$, the magnetic flux lines in this mesoscopic superconductor condense into the vortex cluster at $\kappa_1 = 1.08$ and further form the Abrikosov vortex lattice at $\kappa_1 = 1.58$.

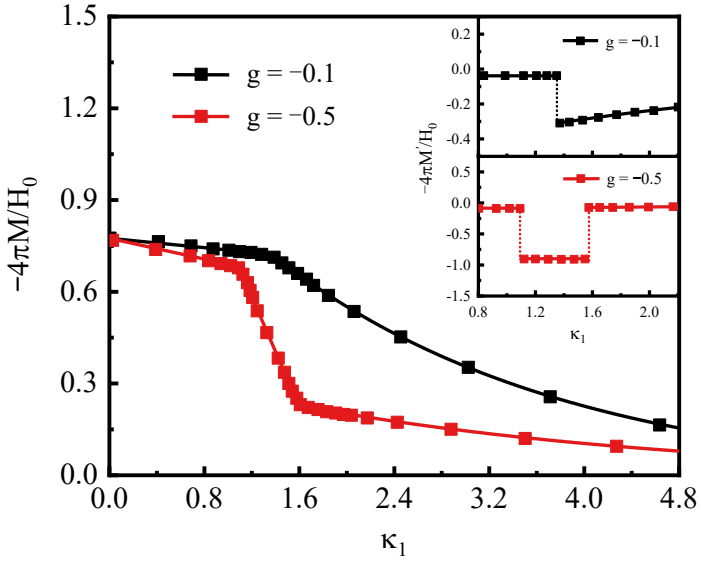

Figure 3: Variations of magnetization M (main) and its first-order derivative M' (inset) with GL parameter κ_1 for the $15\xi_1 \times 15\xi_1$ two-band superconductor in the presence of an isotropic impurity. We set the external magnetic field $H = 0.8H_0$ in the numerical simulations.

With this approach, we can calculate the critical κ_1 for arbitrary value of g and obtain the $g - \kappa_1$ phase diagram as shown in Fig. 4. It can be seen from Fig. 4 that with the increase of the absolute value of g, the vortex cluster phase induced by the attractive interaction from the impurity will gradually appear in the system. Meanwhile, we also see that there exists a critical impurity strength $g_c \approx -0.22$ for the generation of the vortex cluster state in this sample. Thus, the $15\xi_1 \times 15\xi_1$ mesoscopic superconductor will stay in the type-1.5 regime for $|g| > |g_c|$ in the presence of an isotropic impurity. Also see lines 5-18 of the first paragraph on page 9, and lines 1-2 of the first paragraph as well as Fig. 4 on page 10 in the revised version of manuscript.

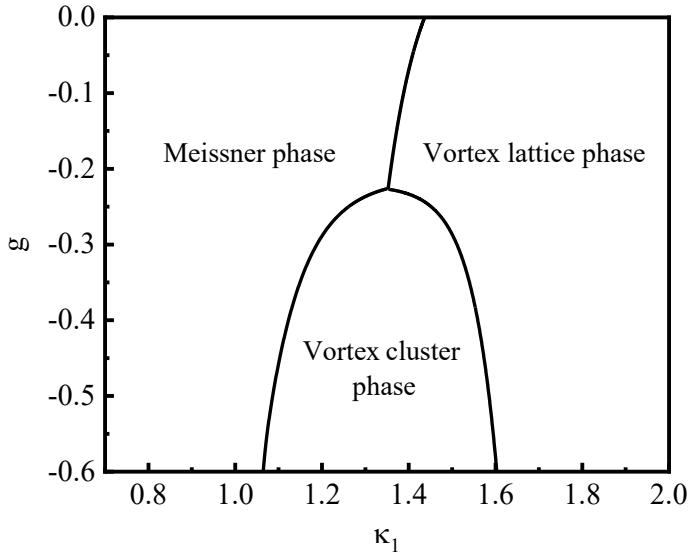

Figure 4: The $g-\kappa_1$ phase diagram of the $15\xi_1 \times 15\xi_1$ two-band superconductor in the presence of an isotropic impurity. We set the external magnetic field $H = 0.8H_0$ in the numerical simulations.

[Q3] Finally, I kindly ask the authors to increase the image resolution and the font size for Fig. 2 and Figs. 4-11. (Quoted from the report of Reviewer 2)

[A3] Following the referee's suggestion, we have significantly improved the image resolution and the font size of Fig. 2 and Figs. 4-11 in the previous manuscript, please see Fig. 3 on page 9 and Figs. 6-13 on pages 11-16 in the revised version of manuscript. We would like to take this opportunity to thank the referee for pointing out this problem to us.